www.czasopisma.pan.pl PAN POLSKA AKADEMIA NAUK www.journals.pan.pl

A R C H I V E S O F M E T A L L U R G Y A N D M A T E R I A L S

Volume 60 2015 Issue 2

DOI: 10.1515/amm-2015-0119

K.S. KIM*,#

ANALYSIS OF DRILLING OF A METAL PLATE WITH PILOT HOLE

ANALIZA WIERCENIA METALOWEJ PŁYTY Z OTWOREM PILOTUJĄCYM

This paper performed a numerical analysis study of the cutting characteristics when drilling a taper hole whose upper and lower diameters are different, that is, a pilot hole. 3-dimensional drilling analysis was performed using a commercial code, and these results were used to determine analytically and compare the cutting temperature, the phenomenon of cutting chip formation, deformation and pressure, etc., for the tools, chips, and specimens during cutting. Also, cutting force and the required energy were calculated and compared. To verify the results of analysis, a cutting dynamometer was used to analyze 3-axis cutting force. Results of analysis showed that the specimen maintained a temperature of approximately 650°, with rapid cooling after chips were formed from the specimen. The tool reached a maximum of 700°, similarly to the chips. It is expected that these results will be utilized to optimize cutting processes and work conditions when drilling holes.

Keywords: Finite element method, Drilling, Pilot hole, Cutting Force, Plastic Strain

1. Governing equations and modeling

The finite element model is composed of a deformable specimen and a rigid tool. The tool penetrates through the specimen at a constant speed and constant feed rate . The commercial Third Wave AdvantEdgeTM Cutting FEM 5.6 have been used to create a coupled thermo-mechanical finite element model of plane-strain orthogonal metal cutting operations. Material is modeled as elastic–plastic, with flow stress being dependent on strain, strain rate and temperature. AdvantEdge is an automated program and it is enough to input process parameters to make a two-dimensional simulation of orthogonal cutting operation. The boundary conditions are hidden to the user. The figure 1 shows the model 1, 2 and 3. This software uses an analytical formulation for material modeling. In a typical machining event, in the primary and secondary shear zones very high strain rates are achieved, while the remainder of the specimen deforms at moderate or low strain rates. In order to account for this, Thirdwave AdvantEdge incorporates a stepwise variation of the rate sensitivity exponent:[1,2]

$$\overline{\sigma} = \sigma_f(\varepsilon^p) \cdot \left(1 + \frac{\dot{\varepsilon^p}}{\dot{\varepsilon_0^p}}\right)^{1/m_1}, \quad if \dot{\varepsilon^p} \leqslant \dot{\varepsilon_0^p} \tag{1}$$

$$\overline{\sigma} = \sigma_f(\varepsilon^p) \cdot \left(1 + \frac{\dot{\varepsilon^p}}{\dot{\varepsilon_0^p}}\right)^{1/m_2} \cdot \left(1 + \frac{\dot{\varepsilon_t}}{\dot{\varepsilon_0^p}}\right)^{1/m_1} \quad f \quad \dot{\varepsilon^p} \leqslant \dot{\varepsilon_t^p} \tag{2}$$

where $\overline{\sigma}$ is the effective von Mises stress, σ_f is the flow stress, ε^p is the accumulated plastic strain, $\dot{\varepsilon_0^p}$ is a reference plastic strain rate, m_1 and m_2 are low and high strain-rate sensitivity exponents, respectively, and $\dot{\varepsilon_t}$ is the threshold strain rate which separates the two regimes. In calculations, a local Newton–Raphson iteration is used to compute $\dot{\varepsilon_0^p}$ according to the low-rate equation, and switches to the high rate equation if the result lies above $\dot{\varepsilon_t}$. σ_f, which is used in Eqs. (1) and (2) is given as:

$$\sigma_t = \sigma_0 \cdot \psi(T) \cdot \left(1 + \frac{\varepsilon^p}{\varepsilon_0^p}\right)^{1/n} \tag{3}$$

where T is the current temperature, σ_0 is the initial yield stress at the reference temperature T_0, ε_0^p is the reference plastic strain, n is the hardening exponent and ψ (T) is the thermal softening factor. In the present study, it is assumed that the tool is not plastifying. Hence, it is considered as rigid. Heat can be transferred to the tool only from the work piece.

2. Modeling and conditions

The specimen used was AISI 1045, most commonly used for mechanical parts. The mechanical characteristics and physical properties of the material are as shown in Table 1. In light of the significant time taken to analyze the specimen, the size was minimized, with both the width and height at 8 mm and the height at 3 mm. As for the pilot holes in the specimen, as shown in Figure 1 and Table 2, the drill diameters for the taper holes on the top plane were 4.5 and 1.0 mm, with the diameter on the bottom plane at a constant 1 mm. The taper angle of

* DIVISION OF MECHANICAL & AUTOMOTIVE ENGINEERING, KONGJU NATIONAL UNIVERSITY, CHEONAN-SI, REPUBLIC OF KOREA

Corresponding author: keysun@kongju.ac.kr

the holes were 60° and 0° (vertical), and to aid the reader's understanding, each of the work conditions were represented by names in Table 2. The material of the tool used was cemented carbide, which is widely and commonly used. [3] A commercial drill without surface coating was used. A twist drill with a 4.5 mm diameter was used, and the angles and dimensions are shown in figure 1. Next, the circumferential speed was 200 m/min, with a rotation speed of 3,000 rpm, a constant feedrate of 0.3 mm/rev, and an outside temperature of 20°[4]. Analysis was performed in 3 dimensions to determine chip shape, 3-component cutting force, and required power in 3D. Chip shape analysis was performed as drilling progressed. The analytical mesh had 3 dimensions with 120,000 rods, divided into triangular elements with 6 nodal points, as shown in Figure 2. Meanwhile, to verify the results of analysis, a cutting dynamometer was used to analyze 3-axis cutting force. The dynamometer used was from Kistler Type 2825A of Germany, and the drilling tool tested was prepared to be identical to the analysis model, as shown in Fig. 9 [5,6].

TABLE 1

The mechanical properties of material

Spec.	Unit	AISI 1045
Tensile Strength	MPa	670
Yield Strength	MPa	450
Modulus of elasticity	GPa	195
Hardness	H_B	197
Density	g/cm^3	7.75

TABLE 2

The model name of specimen

Model name	Base Hole (Fig.1 D_b)	Pilot Hole (Fig.1 D_t)	Taper Angle	Tool Dia.
Model-1	0 (solid)	0 mm(solid)	0°	4.5 mm
Model-2	Dia. 1 mm	Dia. 1.0 mm	0°	
Model-3	Dia. 1 mm	Dia. 4.5 mm	60°	

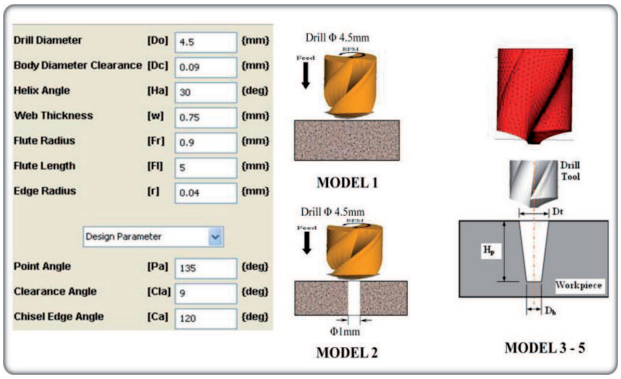

Fig. 1. Geometry of specimen and cutting path

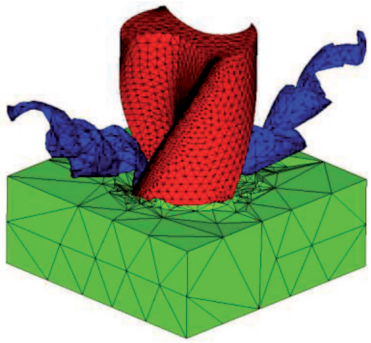

Fig. 2. The mesh generation

3. The results of analysis and discussion

Figure 3 shows the analysis results for the cutting chip formation process. Analyzing Figure 3(a) which is the cutting result for Model-1, because a 2-blade drill is used, plasticity begins to occur from the 2 points in the middle where the end of the blade begins cutting initially. In (b), general breaking occurs, and the chip begins to form. Next, in (c), the chip is formed in a straight line for about 1cm, and, in (e), the chip begins to curl, completing the formation of the shape. Meanwhile, the analysis of the results described pilot holes, while the initial (a) is similar, in (b), unlike in model-1, cutting occurs without breaking. Analyzing the following processes from (c) to (d), whereas in Figure 3, plastic deformation occurs rather than cutting at the center of the drill, in model-2, because a hole has already been made in the center, cutting occurs only, without plastic deformation, causing a regular chip formation shape. Figure 4 shows the temperatures that occur during cutting of the specimens. It can be seen in (a) that the highest temperatures occur at the end of either end of the drill, reaching a maximum of 700°. Next, the specimen maintained a temperature of approximately 650°, excluding the cutting end, with rapid cooling after chips were formed from the specimen. This is a high temperature than can cause the hardness of the specimen to change, therefore measures preventing additional rises in history must be considered during cutting. Next, Figure 4(c) is a graph calculating the average temperature increase at the ends of the blade of the drill tool over a very short period until 3 revolutions. It was seen that the temperature increases rapidly until 0.6 ms, reaching the maximum temperature. Next, the mises stress, shear stress and pressure analysis results for the tool during cutting were shown in Figures 5. It was seen that significant stress was concentrated at the end of the blade of the tool, with maximum stress occurring at point P of (a). It is thought that prolonged use will result in drill blade wear here. The pressure in (c) shows tendencies similar to stress. Meanwhile, Fig. 6 shows the plastic flow speed of the material during cutting. A fast flow of approximately 200m/min was shown at the end of the chip, with the maximum value for plastic strain occurring at the point where cutting occurred. Meanwhile, the cutting power and energy requirements for each of the 3 axes during drill cutting were analyzed. Figure 7-9 shows the analysis time real domain, which has been fitted to a cubic polynomial curve. First, whereas in Figure 7, the z-axis principal cutting

power is approximately 100N, the cutting power of axes X and Y were insignificant. A tendency for cutting power to increase initially, then decrease with plasticity, then increase as the chip grows was seen. The Z-axis cutting force and temperature increase graphs were shown to be similar. Next, the change in cutting force according to increasing angle of pilot hole was compared with Z-axis cutting force, while up to 100N acts on model-1 without base holes, initial cutting power was reduced significantly and became irregular as the angle of pilot hole gradually increased. It is thought that the reason for this is non-continuous chip discharge. Meanwhile, the results of analysis of the energy required as cutting force increases are shown in Figure 8-9. It was seen that up to 670W was required. Lastly, the results of 3-axis cutting power measurements using a cutting dynamometer to verify the analysis are shown in Figure 11. As can be seen, whereas some differences are seen

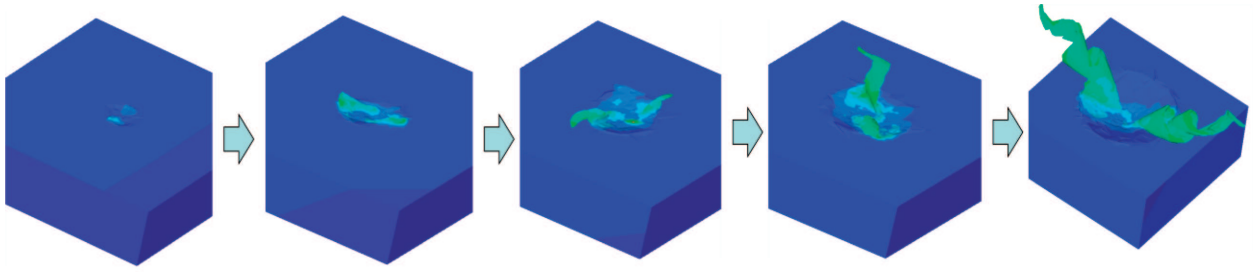

(a) 1st revolution (b) 2nd revolution (c) 3rd revolution (d) 4th revolution (e) 10th revolution

Fig. 3. Chip curve deformation according to revolution

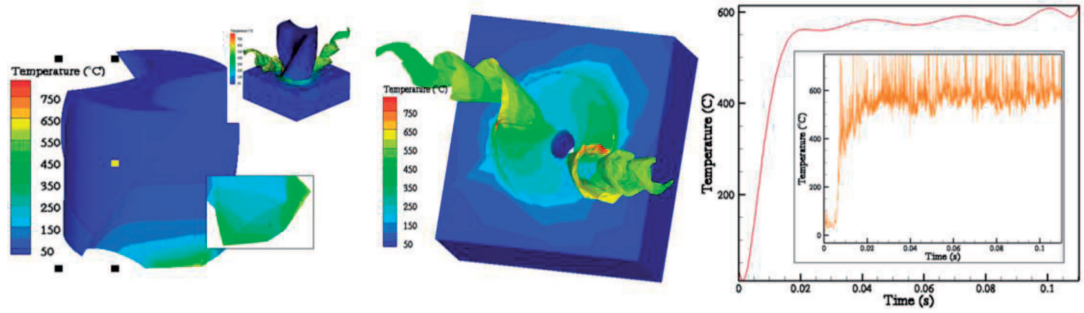

(a) the tool (b) the specimen (c) the average temperature

Fig. 4. Temperature distribution during cutting operation

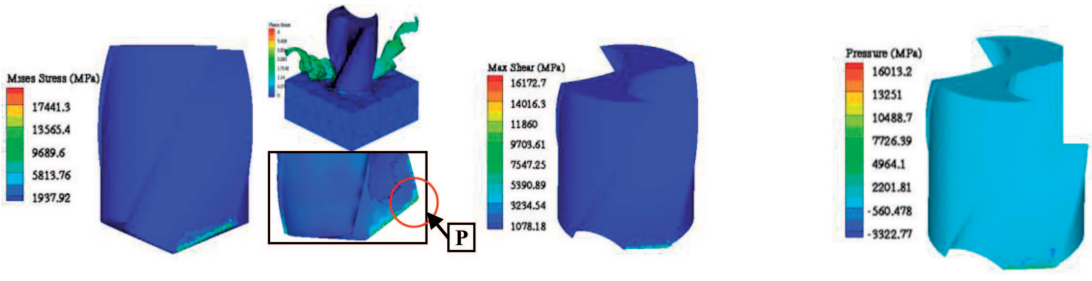

(a) mises Stress of tool (b) shear stress (c) pressure

Fig. 5. Stress and pressure during cutting operation

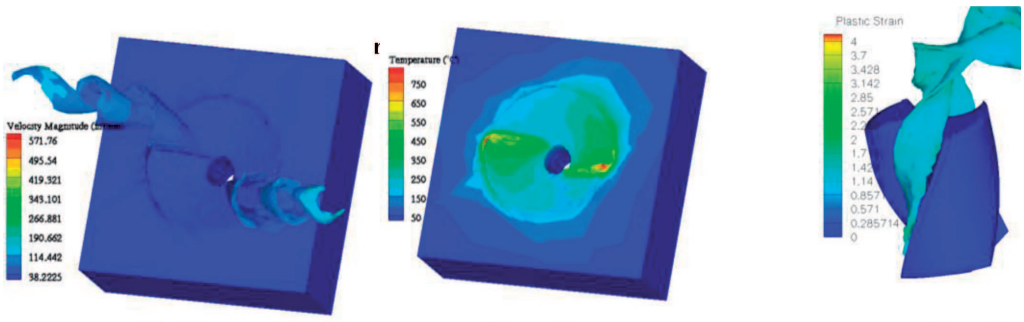

(a) chip (b) specimen (c) tool

Fig. 6. Strain flow during cutting operation

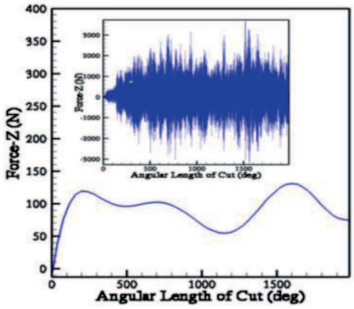

Fig. 7. Force-Z component

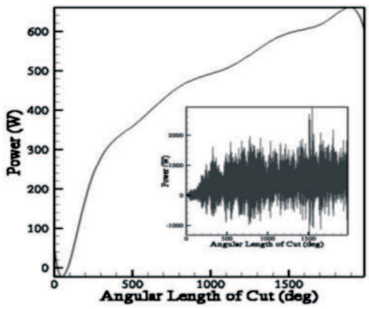

Fig. 8. Cutting power

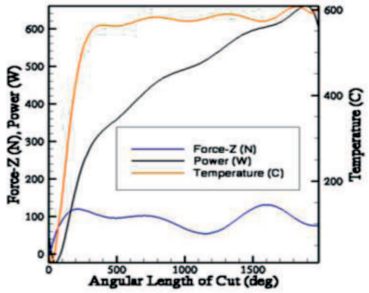

Fig. 9. Force-Z Vs. power Vs. temp.

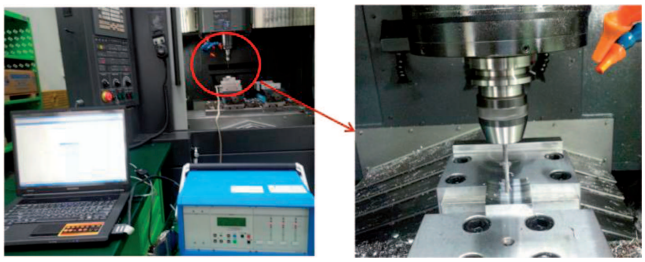

Fig. 10. The experimental configuration for measuring cutting force

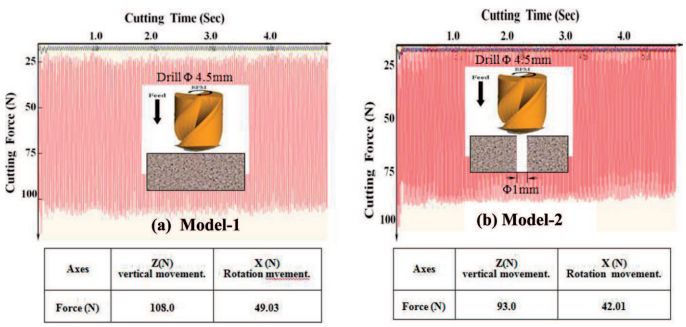

Axes	Z(N) vertical movement.	X (N) Rotation movement.
Force (N)	108.0	49.03

Axes	Z(N) vertical movement.	X (N) Rotation movement.
Force (N)	93.0	42.01

Fig. 11. Force -Z component

in the initial stages of cutting, overall cutting force was shown to be similar. As for the principal cutting power on the Z-axis, at 108N, the difference from the result of analysis was 10%. Picture of the cutting chip during cutting operation are shown in Figure 12 and overall chip deformation was shown to be similar as the results of chip analysis (Figure 3). Therefore it is confirmed that the results of analysis have sufficient value as design parameters.

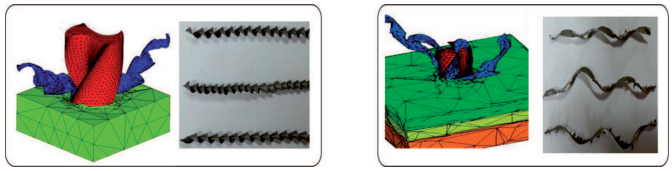

Fig. 12. Force -Z component

4. Conclusion

This study has performed a numerical analysis on the cutting characteristics when drilling pilot holes, and has drawn the following conclusions. First, the cutting temperature, the phenomenon of cutting chip formation, deformation and pressure, etc., for the tools, chips, and specimens during cutting were determined analytically and compared to determine the design variables. It was possible to analytically examine the manner in which the shape of the chip at the end of the tool changes, which is something that cannot actually be measured. Next, cutting force and the required energy were calculated and compared. Meanwhile, results of 3-axis cutting force measurements using a cutting dynamometer to verify the results of analysis differed 10% fom the analysis. Therefore it is confirmed that the results of analysis have sufficient value as design parameters. It is expected that these results will be useful in the future in the selection of cutting processes and equipment for drilling.

REFERENCES

[1] P. Majumdar, R. Jay, S. Ganesan, Finite element analysis of temperature rise in metal cutting process, Applied Thermal Engineering **25**, 14-15, 2039-2495 (2005).

[2] J.-W. Youn, H.-S. Kim, A Study on the Effectiveness of Finite Element Method in Orthogonal Cutting, KSMTE **19**, 1, 42-49 (2010).

[3] M.-Ch. Kang, J.-Y. Heo, Y.-K. Jeong, A. Busnaina, Machinability Evaluation of Hybrid Ti©üAlN Ceramic Composites with Conductivity in Micro Electrical Discharge Drilling Operation, J. of Korean Powder Metallurgy Institute **20**, 4, 285-290 (2013).

[4] J. Thila1a, B. Haddaga, M. Nouaria, L. Papillona, Experimental and analytical analyses of the cutting process in the deep hole drilling with BTA (Boring Trepanning Association) system, Mechanics & Industry **14**, 06, 413-429 (2013).

[5] Y.M. Lee, T.S. Song, B.K. Shim, Analysis of the Up End Milling Process by Transforming to the Equivalent Oblique Cutting Model, KSMPE **2000**, 5, 902-906 (2000).

[6] T.-J. Je, Ch.-E. Kim, H.-J. Choi, E.-Ch. Jeon, M.-Ch. Kang, Comparison of Machinability Between PCD Tool and SCD Tool for Large Area Mirror Surface Machining Using Multi-tool by Planer, J. of Korean Powder Metallurgy Institute **20**, 4, 297-301 (2013).

Received: 20 November 2014.